JOURNAL OF GUIDANCE, CONTROL, AND DYNAMICS
Vol. 39, No. 8, August 2016

Spacecraft Rendezvous by Differential Drag Under Uncertainties

Leonel Mazal,* David Pérez,* and Riccardo Bevilacqua†
University of Florida, Gainesville, Florida 32611
and
Fabio Curti‡
University of Rome "La Sapienza", Rome 00138, Italy

DOI: 10.2514/1.G001785

At low Earth orbits, differentials in the drag forces between spacecraft can be used for controlling their relative motion in the orbital plane. Current methods for determining the drag force may result in errors due to inaccuracies in the density models and drag coefficients. In this work, a methodology for relative maneuvering of spacecraft based on differential drag, accounting for uncertainties in the drag model, is proposed. A dynamical model composed of the mean semimajor axis and the argument of latitude is used for describing long-range maneuvers. For this model, a linear quadratic regulator is implemented, accounting for the uncertainties in the drag force. The actuation is the pitch angle of the satellites, considering saturation. The control scheme guarantees asymptotic stability of the system up to a certain magnitude of the state vector, which is determined by the uncertainties. Numerical simulations show that the method exhibits consistent robustness to accomplish the maneuvers, even in the presence of realistic modeling of density fields, drag coefficients, the corotation of the atmosphere, and zonal harmonics up to J_8.

Nomenclature

A_i	=	cross-sectional area of the surface i of the spacecraft, m^2
$\boldsymbol{a}_D$	=	drag force per unit mass, km/s^2
$\bar{a}$	=	mean semimajor axis, km
C_B	=	spacecraft's ballistic coefficient, m^2/kg
C_{D_i}	=	drag coefficient of the surface i of the spacecraft
$\bar{i}$	=	mean inclination, rad
m	=	spacecraft's mass, kg
P	=	positive-definite matrix, solution of the algebraic Riccati equation
$\boldsymbol{r}$	=	spacecraft's inertial position, km
S_i	=	surface of the face i of the spacecraft, m^2
$\boldsymbol{v}$	=	spacecraft's inertial velocity, km/s
$\boldsymbol{v}_{\text{atm}}$	=	Earth atmosphere's inertial velocity, km/s
$\boldsymbol{v}_{\text{rel}}$	=	velocity vector of the spacecraft relative to the atmosphere, km/s
β	=	attitude angle, deg
η	=	uncertainties (modeling errors) in the input, 1/km
θ	=	argument of latitude, rad
μ	=	Earth's gravitational parameter, km^3/s^2
ν	=	control input to the system, 1/km
ρ	=	Earth's atmospheric density, kg/m^3

I. Introduction

IN LOW Earth orbits (LEOs), the drag force constitutes one of the main perturbations affecting satellite dynamics. The specific force (force per unit mass) $\boldsymbol{a}_D$ generated by the drag force is usually modeled as ([1] p. 549)

$$\boldsymbol{a}_D = -\rho \boldsymbol{v}_{\text{rel}} \| \boldsymbol{v}_{\text{rel}} \| C_B \tag{1}$$

where $\boldsymbol{v}_{\text{rel}}$ denotes the velocity vector of the satellite relative to the atmosphere, ρ represents the atmospheric density, and C_B is the ballistic coefficient. The ballistic coefficient is defined as

$$C_B \triangleq \frac{1}{2m} \sum_i^N C_{D_i} A_i \tag{2}$$

where A_i stands for the cross-sectional area of the ith surface impinged by the particles, C_{D_i} is the corresponding drag coefficient, and m denotes the mass of the spacecraft. Equation (1) shows that $\boldsymbol{a}_D$ always acts in the direction opposed to the vector $\boldsymbol{v}_{\text{rel}}$, which represents the inertial velocity of the satellite relative to the atmosphere. Since the atmosphere inertial velocity is usually a small component compared to the inertial velocity of a LEO satellite, it is frequently neglected for theoretical developments, leading to use of the inertial velocity of the satellite $\boldsymbol{v}$ instead of $\boldsymbol{v}_{\text{rel}}$ in Eq. (1). Under this assumption, drag forces cannot have components perpendicular to the instantaneous plane of motion. This is a significant limitation for the use of drag to maneuver. Yet, within the plane of motion, certain relative maneuvers can be achieved by use of drag only, reducing the propellant needs in certain missions [2,3].

The main effect of the drag force is reducing the semimajor axis and eccentricity of the orbit. If the variables of Eq. (1) are judiciously exploited, relative accelerations between two or more satellites can be generated, such that they are steered toward relative states desirable for specific multiple-satellite applications. This idea is usually termed differential-drag (DD) maneuvering. In recent years, the use of DD for satellite relative maneuvers has been actively investigated due to its potential for reducing the propellant needs in formation flying and cluster flight missions. Yet, one should keep in mind that DD maneuvers might increase the orbital decay of the satellites if the implemented controllers require high values of $\boldsymbol{a}_D$. Other factors limiting the use of differential drag are the vanishing effects of the drag force at altitudes above 600 km and the time required to conduct a maneuver, which could be weeks or months.

Leonard et al. [4,5] derived a control scheme that used drag plates acting at either maximum or minimum drag. To that end, the in-plane dynamics was modeled with the Clohessy–Wiltshire equations [6], and the density was assumed constant. Carter and Humi [7] derived linearized equations of relative motion that included effects caused by drag, assuming a drag force model proportional to the square of the velocity. Kumar and Ng [3] extended the work by Leonard et al. [4,5] to consider other acting perturbations, erroneous measurements, and intersatellite distances slightly larger than those considered by

Received 13 October 2015; revision received 5 March 2016; accepted for publication 6 March 2016; published online 18 April 2016.

*Postdoctoral Associate, Mechanical and Aerospace Engineering, MAE-A Building, Room 211. Professional Member AIAA.
†Associate Professor, Mechanical and Aerospace Engineering, MAE-A Building, Room 308. Senior Member AIAA.
‡Associate Professor, School of Aerospace Engineering. Senior Member AIAA.

Leonard et al. but still in the order of magnitude of a few tens of kilometers.

Bevilacqua and Romano [8] and Bevilacqua et al. [9] used the linear formulation obtained by Schweighart and Sedwick [10] to derive a DD-based control algorithm for steering the in-plane relative coordinates to zero. They assumed a constant density and actuation provided by drag plates with two possible configurations: parallel or perpendicular to the velocity vector, thus providing minimum or maximum drag force, respectively. Based on the Schweighart–Sedwick equations [10] and the same aforementioned drag-plates actuation, Pérez and Bevilacqua [11] removed the assumption on constant atmospheric density and proposed an adaptive Lyapunov-based controller to perform rendezvous between two spacecraft. Moreover, an analytical expression for a critical value of the relative acceleration due to drag was proposed. The relative acceleration due to drag must be above this value to ensure convergence of the maneuver. Ben-Yaacov and Gurfil used DD to perform relative maneuvers for cluster-keeping purposes [12] and developed a controller based on the nonlinear dynamics of the relative orbital elements (ROEs) [13]. The linearized equations of motion of the ROEs accounting for secular J_2 effects and DD were derived by Schaub in [14]. Harris and Açkmeşe [15] applied optimal control for DD-based maneuvers. Dell'Elce and Kerschen [16] used pseudo-spectral methods and model predictive control for planning and effectuating rendezvous maneuvers. The control input was a torque exerted onto a reaction wheel that modified the attitude of the satellite, thereby modifying the acceleration due to drag exerted onto the satellites. Moreover, Dell'Elce et al. [17,18] proposed a robust optimal control approach for DD-based rendezvous maneuvers.

So far, the research in this area has been mainly oriented to close-proximity maneuvers, whereas the potential of differential-drag-based maneuvers can go beyond close-proximity operations. Indeed, the ORBCOMM constellation [19] uses differential drag, in an open-loop manner, to control the relative phase angles of the satellites. Moreover, Finley et al. [2] proposed to use DD to separate in phase a number of satellites that were initially in close proximity. One could also envision applications that require us to guide satellites, which are initially separated by large distances (order of magnitude of ~1000 km) in the same orbital plane, along trajectories that drive them into close-proximity configurations. For this purpose, DD can be also used, enabling reductions in the propellant requirements.

One of the main difficulties of designing differential-drag maneuvers is the inherent uncertainties existing in some of the quantities in Eq. (1). The models of the Earth's atmospheric density field, as well as the drag coefficient values associated to various satellite geometries, can be inaccurate [20], leading to uncertainties in the effects of differential-drag-based maneuvers. Hence, when designing differential-drag-based maneuvers, these uncertainties should be accounted for.

One of the goals of this work is to design differential-drag cooperative maneuvers by explicitly considering uncertainties in the drag models, which at the best knowledge of the authors has not received much attention. These maneuvers are aimed at steering the satellites from given initial conditions to close-proximity configurations oriented to a rendezvous. Inspired by the flourishing CubeSat format, this work assumes that the satellite geometries are rectangular parallelepipeds that can change their pitch angles in a continuous manner, hence varying the cross-sectional area and the resulting differential-drag accelerations.

The proposed approach aims at dealing with the uncertainties in the atmospheric density models and in the ballistic coefficients. To derive the control laws of the maneuvers, the problem is formulated using a linearized relative motion representation, based on orbital elements. The linearization is based on the main assumption that the difference in mean semimajor axes between the two satellites is small compared to the mean semimajor axes values. Unlike other linearized formulations [6,10], this model allows large distances between the satellites, as long as both mean semimajor axes are kept close one to each other. In this manner, one can consider initially large phase-separations between the satellites and drive them into close-proximity configurations. In this context, a linear quadratic regulator (LQR) is proposed. Moreover, an analysis of the convergence of the system driven by the proposed LQR controller in the presence of bounded uncertainties is presented. This leads to determine gains ensuring that the system still converges, under these uncertainties, up to a certain norm of the state vector. Since the cross-sectional area of the satellites is limited, an assessment of the system under saturation is provided, showing that convergence is still achieved.

The approach presented is tested using maneuver simulations that include: space- and time-varying density using NRLMSISE-00, including the influence of the solar and geomagnetic activity; the effects of the rotation of atmosphere on the drag force; a realistic model for the drag coefficient that takes into account the composition of the surfaces, their orientation, and the thermal difference between the surfaces and the atmosphere; and a gravitational geopotential due to zonal harmonics up to J_8. The effects of these factors on the resulting maneuvers are studied by running different scenarios with different combinations of these factors.

The advancements on the state of the art in this work are as follows:

1) The first advancement is the development of an LQR approach for DD-based maneuvering that guarantees convergence up to a bound around the desired final state under uncertainties in the density and the drag coefficient.

2) For the developed dynamical model, the control law is augmented with a saturation function, still providing convergence.

3) Validation of the LQR approach using numerical simulations for a long-range rephasing maneuver, including realistic density, variable drag coefficient, corotating atmosphere, and zonal harmonics up to J_8.

The remainder of the paper is organized as follows: Sec. II introduces the geometrical setup assumed to tackle the problem; Sec. III addresses the problem with a formulation based on orbital elements, deriving an LQR controller; and Sec. IV shows numerical simulations supporting the theoretical statements. Finally, concluding remarks are provided in Sec. V.

II. Description of the Problem

Let two satellites, the chaser and the target, be in coplanar circular orbits. The main goal of this work is to derive DD-based closed-loop controllers that steer the satellites to an encounter. These maneuvers will be performed by varying the drag force generated on either satellite, with no thrust usage.

Motivated by the rapid increase in the number of missions composed of CubeSats, this work assumes that the satellite geometries are rectangular parallelepipeds, such as the one illustrated in the three-dimensional (3-D) view of Fig. 1. In this paper, these bodies are endowed with one rotational degree of freedom, with the axis of rotation always perpendicular to the plane which is depicted as a dashed-dot line in the 3-D view of Fig. 1. The input considered for the control laws is the attitude of the satellite parameterized by the angle β, according to Fig. 1. To measure β, define a line lying on the orbital plane, perpendicular to the inertial velocity vector of the satellite $\boldsymbol{v}$, such as the dashed line illustrated in the two-dimensional (2-D) view and orbital view of Fig. 1. β is measured from the aforementioned line toward the satellite velocity vector. In Fig. 1, S_1 and S_2 denote the surfaces perpendicular to the plane of motion, whereas the face S_3 remains parallel to the plane of motion. For the forthcoming analytical developments, the velocity of the atmosphere is neglected, but it will then be incorporated in numerical simulations to assess the effects on the developed controller. Hence, the total product of the drag coefficient by cross-sectional area is given by

$$\sum_{i=1}^{2} S_i C_{D_i} = C_{D_1} S_1 |\cos\beta| + C_{D_2} S_2 |\sin\beta| \tag{3}$$

Changing β modifies the cross-sectional areas, and consequently the magnitude of the exerted acceleration $\boldsymbol{a}_D$. Due to the periodicity of the cross-sectional areas with β, for the purposes of this work, β can be restricted to the range $\beta \in [0\ \text{deg}, 90\ \text{deg}]$, which allows us to remove the absolute value operator from Eq. (3).

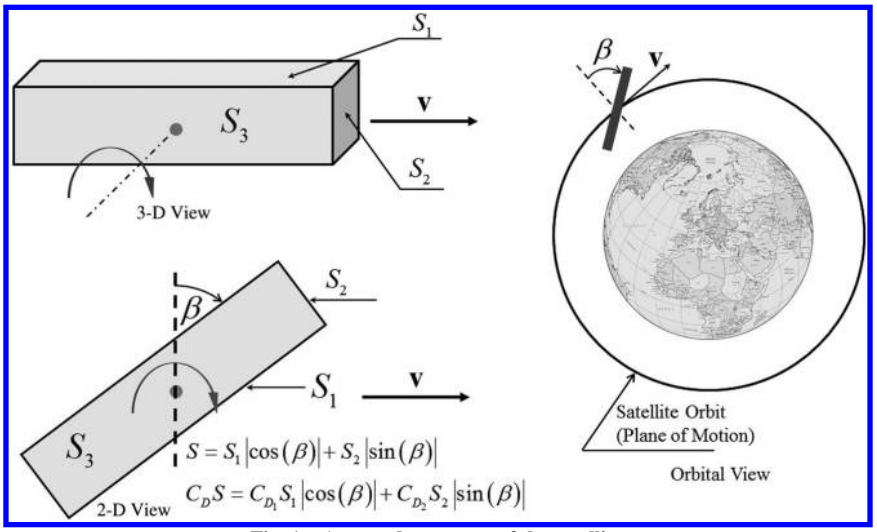

Fig. 1 Assumed geometry of the satellite.

Because of the general lack of knowledge on the drag coefficient behaviors, for the purpose of controller development, the drag coefficient will be assumed to be a constant value and equal for both satellites, since the geometries are alike. However, since a constant value might be an erroneous modeling, the effects on the dynamics due to uncertain variations of the real values with respect to the assumed constant values will be theoretically assessed. Hence, assuming $C_{D_i} = C_D$ and is constant, Eq. (3) can be reformulated as

$$\sum_{i=1}^{2} C_{D_i} S_i = C_D S = C_D S_0 \cos(\beta - \psi) \tag{4}$$

where $S_0 = \sqrt{S_1^2 + S_2^2}$, and $\psi = \arctan(S_2/S_1)$. It can be seen that

$$\sum_{i=1}^{2} C_{D_i} S_i$$

has a maximum at $\beta = \psi > 0$ and a minimum at $\beta = 90$ deg. Hence, for the purposes of this work, the range of β can be restricted even more: $\beta \in [\psi, 90 \text{ deg}]$.

III. Rephasing Maneuvers Under Uncertainties

This section presents an approach to drive two satellites that are initially in circular orbits in the same orbital plane but separated in phase (i.e., with different arguments of latitude) toward a close-proximity configuration. This configuration is attained by matching the mean semimajor axes $\bar{a}$ of the satellites and the mean argument of latitude $\bar{\theta}$. Notice that, for initially circular orbits (very low eccentricities), neither the Earth's oblateness nor drag effects increase the mean eccentricities, i.e., the orbits will remain circular [in fact, drag reduces the eccentricity of orbits ([1] p. 671)]. Hence, matching $\bar{a}$ and $\bar{\theta}$ brings the two satellites into a close-proximity configuration.

A. Dynamic Model

Let $\bar{a}, \bar{e}, \bar{i}, \bar{\omega}$, and $\bar{M}$, respectively, denote the mean semimajor axis, eccentricity, inclination, argument of perigee, and mean anomaly. Under the influence of drag and the first term of the gravitational geopotential due to zonal harmonics J_2, the time variation of the mean argument of perigee $\bar{\omega}$ and the mean anomaly $\bar{M}$ are, respectively, given by [21]

$$\dot{\bar{\omega}} = \frac{3}{4} J_2 \bar{n} \left(\frac{R_{\text{eq}}}{\bar{p}}\right)^2 (5\cos^2 \bar{i} - 1) \tag{5}$$

$$\dot{\bar{M}} = \bar{n} + \frac{3}{4} J_2 \bar{n} \left(\frac{R_{\text{eq}}}{\bar{p}}\right)^2 \sqrt{1 - \bar{e}^2} (3\cos^2 \bar{i} - 1) \tag{6}$$

where $\bar{p}$ and $\bar{n}$ denote the parameter (semilatus rectum) of the orbits and the mean motion, respectively; and R_{eq} represents the mean equatorial radius of the Earth.

The argument of latitude θ is defined as $\theta \triangleq \omega + f$, where f denotes the true anomaly. Assuming circular orbits, the variation of the mean argument of latitude can be modeled as

$$\dot{\bar{\theta}} = \dot{\bar{M}} + \dot{\bar{\omega}} \quad = \sqrt{\frac{\mu}{\bar{a}^3}} + \frac{3}{4} J_2 \sqrt{\frac{\mu}{\bar{a}^3}} \left(\frac{R_{\text{eq}}}{\bar{a}}\right) (8\cos^2 \bar{i} - 2) \tag{7}$$

To model the rate of change of the mean semimajor axis, we use the Gauss variational equations (GVEs) and the premise that "the effects of the control vector $\boldsymbol{u}$ is assumed to have the same effect on the mean orbit elements as it has on the osculating orbit elements," as mentioned by Schaub and Alfriend [22]. In this work, the vector $\boldsymbol{u}$ will be generated using drag forces. Hence, the effects of the drag on the mean semimajor axis will be approximated by the effect that the same drag would generate on the corresponding osculating semimajor axis. This approximation has been proposed and assessed in a few papers [21,23,24], showing its validity.

Using the GVEs resolved in tangential and normal axes ([25] p. 489), the time variation of the semimajor axis a is formulated as

$$\dot{a} = \frac{2a^2 v}{\mu} \Gamma_t \tag{8}$$

where $v \triangleq \|\boldsymbol{v}\|$, and Γ_t represents the disturbance acceleration component along the inertial velocity vector. The perturbation due to J_2 has no effect on $\bar{a}$. Neglecting any motion of the atmosphere and considering Eq. (4), the input Γ_t due to drag is given by

$$\Gamma_t = -\frac{1}{2} \rho v^2 \frac{C_D}{m} S_0 \cos(\beta - \psi) \tag{9}$$

Since, for circular orbits $v = \sqrt{\mu/a}$, introducing Eq. (9) into Eq. (8) and recalling that the rate of change of the mean semimajor axis due to drag will be approximated by the rate of change that the drag would induce onto the osculating semimajor axis [22], $\dot{\bar{a}}$ is approximated by

$$\dot{\bar{a}} = -2\sqrt{\mu \bar{a}} \rho \frac{C_D S_0}{2m} \cos(\beta - \psi) \tag{10}$$

The quantity $C_D S_0/(2m)$ will be denoted by C_{B0} and will be considered constant for the development of the control law. However,

in reality, the real drag coefficient is affected by variations of the attitude, temperature, and chemical composition of the surface of the spacecraft and the environment [26–28]. The effects of these uncertain variations in the performance of the control law will be addressed in Sec. III.C.

Recall that, under J_2 and drag influence, the mean inclination $\bar{i}$ remains constant; thus, it actually represents a parameter. It is important to mention that the reduced state $[\bar{\theta}, \bar{a}]^\top$ represents only the in-plane motion.

The relative orbital elements are defined as

$$\Delta\bar{\theta} \triangleq \bar{\theta}_C - \bar{\theta}_T \tag{11}$$

$$\Delta\bar{a} \triangleq \bar{a}_C - \bar{a}_T \tag{12}$$

In Eqs. (11) and (12), as well as for the remainder of the paper, the subindices $(\cdot)_C$ or $(\cdot)_T$ refer to the parameter or variable $(\cdot)$ associated to the chaser or target, respectively. The lack of a subindex in certain expressions indicates that the expression is valid for either spacecraft indistinctly.

Generally speaking, in multiple-satellite missions that involve coordinated relative motion, the mean semimajor axes should be close on to each other, i.e., $|\bar{a}_C - \bar{a}_T|/\bar{a}_T \ll 1$; otherwise, there would be high natural drift rates that could rapidly dismantle any desired configuration.

Consider a virtual satellite 0 in a circular orbit with the constant mean semimajor axis $\bar{a}_0$ (i.e., unaffected by drag). Assume $\bar{a}_0$ is sufficiently close to $\bar{a}_C$ and $\bar{a}_T$, and the inclination $\bar{i}_0 = \bar{i}_C = \bar{i}_T = \bar{i}$. Considering Eq. (7), the difference in the rate of change of the arguments of latitude between the satellites C and 0 can be linearized as

$$\dot{\bar{\theta}}_C - \dot{\bar{\theta}}_0 \simeq \left.\frac{\partial\dot{\bar{\theta}}}{\partial\bar{a}}\right|_{\bar{a}=\bar{a}_0} (\bar{a}_C - \bar{a}_0) \tag{13}$$

The difference in the rate of change of the arguments of latitude between the satellites T and 0 can be obtained in a similar manner. Finally,

$$\Delta\dot{\bar{\theta}} = \dot{\bar{\theta}}_C - \dot{\bar{\theta}}_0 - (\dot{\bar{\theta}}_T - \dot{\bar{\theta}}_0) = -P_0\Delta\bar{a} \tag{14}$$

where

$$P_0 \triangleq \sqrt{\mu}\left[\frac{3}{2}\frac{1}{\bar{a}_0^{5/2}} + \frac{21}{8}\frac{J_2 R_{\text{eq}}^2(8\cos^2\bar{i} - 2)}{\bar{a}_0^{9/2}}\right] \tag{15}$$

Equation (14) represents the evolution of the relative mean argument of latitude as a function of the mean relative semimajor axis. Due to the linearizations, this equation remains valid as long as the mean semimajor axes of the chaser and target remain sufficiently close to $\bar{a}_0$. As previously stated, because of the coordinated motion, $\bar{a}_C$ and $\bar{a}_T$ are expected to remain relatively close one to each other; otherwise, there would be a high drift hindering any possible coordinated maneuver. Moreover, during the maneuvers, the variations of the mean semimajor axes due to drag are expected to be sufficiently small, holding the linearizations valid, i.e.,

$$\frac{|\bar{a}(t) - \bar{a}_0|}{\bar{a}_0} \ll 1$$

These assumptions will be validated during the extensive numerical simulations presented in Sec. IV.

To obtain $\Delta\dot{\bar{a}}$, considering Eq. (10) and taking the zeroth-order Taylor expansion about $\bar{a} = \bar{a}_0$ yields

$$\Delta\dot{\bar{a}} = -2\sqrt{\mu\bar{a}_0}(\rho_C u_C - \rho_T u_T) \tag{16}$$

where

$$u_C \triangleq C_{B0}\cos(\beta_C - \psi) \qquad u_T \triangleq C_{B0}\cos(\beta_T - \psi) \tag{17}$$

Defining $\boldsymbol{w} \triangleq [\Delta\bar{\theta}, \Delta\bar{a}]^\top$, the obtained linear system can be written as follows:

$$\dot{\boldsymbol{w}} = \begin{bmatrix} 0 & -P_0 \\ 0 & 0 \end{bmatrix}\boldsymbol{w} + \begin{bmatrix} 0 \\ b \end{bmatrix}(-\rho_C u_C + \rho_T u_T) \tag{18}$$

where $b \triangleq 2\sqrt{\mu\bar{a}_0}$. The dynamical system [Eq. (18)] may be considered linear time invariant (LTI). The input of this system is given by the term $-\rho_C u_C + \rho_T u_T$. Notice that the uncertainties in the densities ρ_C and ρ_T, as well as in the drag coefficient C_D, constitute uncertainties in the input.

B. Controller Derivation

Assuming no constraints on the input, an infinite-horizon LQR approach will be initially implemented. Since the range of $\nu \triangleq -\rho_C u_C + \rho_T u_T$ is limited, a saturation function will be proposed in the sequel, and it will be shown that convergence is still achieved. Recall that, in an infinite-horizon LQR, if $\boldsymbol{w}$ denotes the state vector, the input is given by ([29] chap. 3.3)

$$\boldsymbol{\nu}_{\text{LQR}} = -R^{-1}B^\top P\boldsymbol{w} \tag{19}$$

where P is the matrix that solves the algebraic Riccati equation formulated as

$$A^\top P + PA - PBR^{-1}B^\top P + Q = O \tag{20}$$

For the problem in question, the matrices are given by

$$A = \begin{bmatrix} 0 & -P_0 \\ 0 & 0 \end{bmatrix} \quad B = \begin{bmatrix} 0 \\ b \end{bmatrix} \quad R > 0$$

Q is a positive-definite matrix defined as

$$Q \triangleq \begin{bmatrix} q_1 & 0 \\ 0 & q_2 \end{bmatrix}$$

i.e., $q_1 > 0$ and $q_2 > 0$, P is a positive-definite matrix defined as

$$P \triangleq \begin{bmatrix} \Pi_1 & \Pi_2 \\ \Pi_2 & \Pi_3 \end{bmatrix}, \quad O \triangleq \begin{bmatrix} 0 & 0 \\ 0 & 0 \end{bmatrix}$$

For the discussed problem, P is sought such that the matrix

$$A^* \triangleq A - BR^{-1}B^\top P \tag{21}$$

is Hurwitz, i.e., all the eigenvalues of A^* must have negative real part. Hence, the expressions for the entries of the matrix P are determined as

$$\Pi_1 = \frac{\sqrt{q_1}\sqrt{2P_0\sqrt{q_1R} + q_2 b}}{P_0\sqrt{b}} \tag{22}$$

$$\Pi_2 = -\frac{\sqrt{q_1 R}}{b} \tag{23}$$

$$\Pi_3 = \frac{\sqrt{R}\sqrt{2P_0\sqrt{q_1R} + q_2 b}}{b^{3/2}} \tag{24}$$

and the gain $\boldsymbol{K}$ is

$$\boldsymbol{K} = R^{-1}B^{\top}P = \left[-\sqrt{\frac{q_1}{R}}\sqrt{2\frac{P_0}{b}\sqrt{\frac{q_1}{R}}+\frac{q_2}{b}}\right] \tag{25}$$

With $\boldsymbol{K}$ already computed, then the desired input to the system is

$$\nu_{\text{des}} = -\boldsymbol{K}[\Delta\bar{\theta}, \Delta\bar{a}]^{\top} \tag{26}$$

Now, assuming that

$$(-\rho_C + \rho_T\zeta)C_{B0} \le \nu_{\text{des}} \le (-\rho_C\zeta + \rho_T)C_{B0} \tag{27}$$

where $\zeta \triangleq \cos(\pi/2 - \psi)$, one should find β_C and β_T (the pitch angles of the chaser and target, respectively), such that

$$-\rho_C u_C + \rho_T u_T = \nu_{\text{des}} \tag{28}$$

If the constraints [Eq. (27)] are not satisfied, there are no $\beta_C \in \mathbb{R}$ and $\beta_T \in \mathbb{R}$ that satisfy Eq. (28). This case will be addressed in the sequel.

C. Effects of the Uncertainties in the Implementation

To find β_C and β_T that solve Eq. (28), a model for the atmospheric density must be selected, from which the densities for the chaser and target are, respectively, assumed to be ρ_C^* and ρ_T^*. Similarly, one should also consider a nominal value for the drag coefficient C_D^*, which leads to a nominal value $C_{B0}^* = S_0 C_D^*/(2m)$, yielding assumed $u_C^* = C_{B0}^*\cos(\beta_C - \psi)$ and $u_T^* = C_{B0}^*\cos(\beta_T - \psi)$. Hence, if

$$(-\rho_C^* + \rho_T^*\zeta)C_{B0}^* \le \nu_{\text{des}} \le (-\rho_C^*\zeta + \rho_T^*)C_{B0}^* \tag{29}$$

β_C and β_T are actually found from the equation

$$(-\rho_C^* u_C^* + \rho_T^* u_T^*) = \nu_{\text{des}} \tag{30}$$

However, considering that the models are uncertain, the real densities affecting the spacecraft are given by $\rho_C = \rho_C^* + \delta\rho_C$ and $\rho_T = \rho_T^* + \delta\rho_T$, where $\delta\rho_C$ and $\delta\rho_T$ denote the differences between the real and assumed density for the chaser and target, respectively. Correspondingly, the real values of u_C and u_T are given by $u_C = u_C^* + \delta u_C$ and $u_T = u_T^* + \delta u_T$. Hence, the true input of the system is given by

$$\begin{aligned}\nu_{\text{true}} &= -(\rho_C^* + \delta\rho_C)(u_C^* + \delta u_C) + (\rho_T^* + \delta\rho_T)(u_T^* + \delta u_T)\\ &= \nu_{\text{des}} + \eta\end{aligned} \tag{31}$$

where

$$\eta \triangleq -\rho_C^*\delta u_C + \rho_T^*\delta u_T - \delta\rho_C u_C^* + \delta\rho_T u_T^* - \delta\rho_C\delta u_C + \delta\rho_T\delta u_T \tag{32}$$

For the forthcoming analysis, the respective quantities are considered normalized by the corresponding units; i.e., distances by 1 km, angles by 1 rad, mass by 1 kg, and time by 1 s. To assess the effects on the maneuvers caused by the errors in the density models and drag coefficient, consider the positive-definite function $V = \boldsymbol{w}^{\top}P\boldsymbol{w}$. Considering Eq. (18), its time derivative is then given by

$$\begin{aligned}\dot{V} = 2\boldsymbol{w}^{\top}P[&A\boldsymbol{w} + B(-(\rho_C^* + \delta\rho_C)(u_C^* + \delta u_C)\\ &+ (\rho_T^* + \delta\rho_T)(u_T^* + \delta u_T))]\end{aligned} \tag{33}$$

Introducing Eqs. (26), (30), and (32) yields

$$\begin{aligned}\dot{V} &= 2\boldsymbol{w}^{\top}P[A\boldsymbol{w} + B(\nu_{\text{des}} + \eta)]\\ &= 2\boldsymbol{w}^{\top}P[(A - B\boldsymbol{K})\boldsymbol{w} + B\eta]\\ &= \boldsymbol{w}^{\top}[P(A - B\boldsymbol{K}) + (A - B\boldsymbol{K})^{\top}P]\boldsymbol{w} + 2\boldsymbol{w}^{\top}PB\eta\\ &= -\boldsymbol{w}^{\top}(\boldsymbol{Q} + PBR^{-1}B^{\top}P)\boldsymbol{w} + 2\boldsymbol{w}^{\top}PB\eta\end{aligned} \tag{34}$$

which can be upper bounded by

$$\dot{V} \le \Upsilon(\|\boldsymbol{w}\|) \triangleq -\|\boldsymbol{w}\|^2\lambda_{\min} + 2\|\boldsymbol{w}\|\|PB\|\bar{\eta} \tag{35}$$

where $\bar{\eta} \ge |\eta|$, and $\lambda_{\min} > 0$ denotes the smallest eigenvalue of the symmetric matrix $\Xi \triangleq Q + PBR^{-1}B^{\top}P$. Based on Eq. (32), an upper bound for $|\eta|$ can be formulated as

$$|\eta| \le \bar{\eta} \triangleq 2(\rho_M^* M\delta u^M + u^{*M}\delta\rho^M + \delta\rho^M\delta u^M) \tag{36}$$

where the superscript M indicates that the maximum possible value is taken for the corresponding parameter. Generally speaking, $\bar{\eta}$ could be computed based on the maximum expected errors for a given model of density and a given model of the ballistic coefficient. This will be discussed further in the sequel with specific models.

Considering the errors in the atmospheric density models and in the ballistic coefficients, $\dot{V}$ will be always bounded from the aforementioned by $\Upsilon(\|\boldsymbol{w}\|)$, which is a parabola in $\|\boldsymbol{w}\|$. Its roots are located at $\|\boldsymbol{w}\| = 0$ and

$$\|\boldsymbol{w}\| = 2\frac{\|PB\|}{\lambda_{\min}}\bar{\eta} > 0$$

Hence, as long as

$$\|\boldsymbol{w}\| = 2\frac{\|PB\|}{\lambda_{\min}}\bar{\eta}$$

$\dot{V}$ will be negative, as required for convergence ([30] chap. 4). Since V is positive definite, due to continuity (and as long as $\dot{V} < 0$), eventually, $\|\boldsymbol{w}\|$ becomes

$$2\frac{\|PB\|}{\lambda_{\min}}\bar{\eta}$$

and the decreasing rate of V cannot be guaranteed. Hence, there is interest in reducing the ratio $\|PB\|/\lambda_{\min}$, which is a function of Q and R, to reduce the range in which $\dot{V} < 0$ cannot be guaranteed.

The matrix $\boldsymbol{\Xi} = Q + PBR^{-1}B^{\top}P$ is given by

$$\boldsymbol{\Xi} = \begin{bmatrix}\Xi_1 & \Xi_2\\ \Xi_2 & \Xi_3\end{bmatrix} \tag{37}$$

where $\Xi_1 = 2q_1$,

$$\Xi_2 = -\sqrt{\frac{q_1}{b}}\sqrt{2P_0\sqrt{q_1R} + q_2b} \quad \Xi_3 = 2q2 + \frac{2P_0\sqrt{q_1R}}{b}$$

from which its eigenvalues are computed as

$$\lambda_{\max,\min} = \frac{q_2b + P_0\sqrt{q_1R} + q_1b \pm \sqrt{q_2^2b^2 + 2q_2bP_0\sqrt{q_1R} - q_1q_2b^2 + q_1RP_0^2 + q_1^2b^2}}{b} \tag{38}$$

Hence,

$$\frac{\|PB\|}{\lambda_{\min}} = \frac{\sqrt{\tilde{q}_1+\tilde{q}_2+2P_0/b\sqrt{\tilde{q}_1}}}{\tilde{q}_1+\tilde{q}_2+P_0/b\sqrt{\tilde{q}_1}-\sqrt{(\tilde{q}_1^2+\tilde{q}_2^2)+(P_0/b)^2\tilde{q}_1+2P_0/b\sqrt{\tilde{q}_1}\tilde{q}_2-\tilde{q}_1\tilde{q}_2}} \tag{39}$$

where $\tilde{q}_1 \triangleq q_1/R$ and $\tilde{q}_2 \triangleq q_2/R$. Notice that the right-hand side of Eq. (39) does not depend on q_1, q_2, or R explicitly but on $\tilde{q}_1$ and $\tilde{q}_2$. Moreover, $\|PB\|/\lambda_{\min}$ is a positive function of $\tilde{q}_1$ and $\tilde{q}_2$, which can be selected to reduce $\|PB\|/\lambda_{\min}$ as much as desired while keeping in mind that this affects the required control efforts and might generate saturation in the system. However, the next section shows that, if the system is saturated, it will eventually reach a nonsaturated configuration where Eq. (29) is satisfied, and thus convergence up to

$$\|\boldsymbol{w}\| = 2\frac{\|PB\|}{\lambda_{\min}}\bar{\eta} > 0$$

can be achieved.

D. Saturation

According to the proposed controller, the desired input of the system is given by Eq. (26). On the other hand, the required attitude angles β_C and β_T are computed according to Eq. (30). As previously mentioned, in order to find $\beta_C \in \mathbb{R}$ and $\beta_T \in \mathbb{R}$, inequality (29) must hold. However, for certain values of $\Delta\bar{\theta}$ and $\Delta\bar{a}$, inequality (29) might be not satisfied, and thus there are no valid β_C and β_T satisfying Eqs. (26) and (30). This occurs because the ballistic coefficients of the satellites are limited, whereas the input of a linear controller of the form of Eq. (26) can, theoretically, attain any value.

To address this problem, this work proposes to implement a saturation function. Whenever inequality (29) is not satisfied, the system implements attitudes β_C and β_T such that the maximum or minimum feasible differential-drag acceleration is obtained. It yields

$$\beta_C = \frac{\pi}{2} \quad \text{and } \beta_T = \psi, \qquad \text{if } -\boldsymbol{K}[\Delta\bar{\theta}, \Delta\bar{a}]^\top \geq C_{B0}(-\rho_C^*\zeta + \rho_T^*) \tag{40}$$

$$\beta_C = \psi \quad \text{and } \beta_T = \frac{\pi}{2}, \qquad \text{if } -\boldsymbol{K}[\Delta\bar{\theta}, \Delta\bar{a}]^\top \leq C_{B0}(-\rho_C^* + \rho_T^*\zeta) \tag{41}$$

$$C_{B0}^*(-\rho_C^*\cos(\beta_C-\psi) + \rho_T^*\cos(\beta_T-\psi)) = -\boldsymbol{K}[\Delta\bar{\theta}, \Delta\bar{a}]^\top, \text{otherwise} \tag{42}$$

The goal of this section is to show that the dynamical system given by Eqs. (14) and (16) still converges to the origin if it is driven by the control law stated by Eqs. (40–42). This will be done by depicting the phase portrait of the system and analyzing the resulting trajectories.

Since the atmospheric density certainly depends on the altitude of the satellites, it is necessary to assume a density field model that captures the main density behavior due to changes in the semimajor axes of the satellites. Analytical expressions of the density as a function of the altitude show an exponential decay due to hydrostatic equilibrium. On the other hand, there exist variations of the density due to effects other than altitude, like solar activity, diurnal cycles, etc. Yet, the simplest models tend to average out these variations, showing only variations due to altitude. The forthcoming analysis examines the behavior of the two satellites, under saturation, assuming that the main variations of the density are due to altitude and any other effect is averaged out. Still, the effects due to the expected uncertainties on the dynamics will be addressed. Hence, for the forthcoming analysis, the exponential atmospheric model CIRA-72 published in ([1] p. 564) will be used, as it captures the aforementioned behavior and allows us to keep the math tractable. In this model, the atmospheric density is computed as

$$\rho(h) = \rho_H e^{-h-h_0/H} \tag{43}$$

where ρ_H, h_0, and H denote model parameters that are tabulated in the aforementioned reference for various intervals of altitude h.

Since the orbits are assumed circular (assuming spherical Earth with radius R_{eq}), Eq. (43) can be approximately reformulated as

$$\rho(\bar{a}) = \rho_H e^{-\bar{a}-(h_0+R_{\text{eq}})/H} \tag{44}$$

where the constant h_0 represents the lowest altitude of the interval of interest. Since the mean semimajor axes of the satellites are expected to be sufficiently close, from Eq. (44), ρ_C^* can be modeled as

$$\rho_C^* \simeq \rho_T^* + \left.\frac{\partial\rho}{\partial\bar{a}}\right|_{\bar{a}_T}\Delta\bar{a} = \rho_T^*\left(1-\frac{\Delta\bar{a}}{H}\right) \tag{45}$$

where H is (a single value) selected for the proper range of altitudes. Any density variations due to solar activity would result in time-varying coefficients for the model [Eq. (44)]. Yet, the same relation [Eq. (45)] would be obtained, provided that the semimajor axes of the satellites are sufficiently close. Moreover, notice that, for a constant density model, Eq. (44) is still valid with H that tends to infinity.

To proceed, the region in which Eq. (42) has solutions $\beta_C \in \mathbb{R}$ and $\beta_T \in \mathbb{R}$ is first determined. From inequality (29) and introducing Eq. (45), this region is obtained as

$$S_U\Delta\bar{\theta} + M_U \geq \Delta\bar{a} \geq M_L + S_L\Delta\bar{\theta} \tag{46}$$

where

$$S_U \triangleq \frac{-k_1}{k_2 + (C_{B0}^*/H)\rho_T^*} > 0 \tag{47}$$

$$S_L \triangleq \frac{-k_1}{k_2 + (C_{B0}^*/H)\zeta\rho_T^*} > 0 \tag{48}$$

$$M_U \triangleq \frac{(1-\zeta)C_{B0}}{k_2/\rho_T^* + C_{B0}^*/H} > 0 \tag{49}$$

$$M_L \triangleq -\frac{C_{B0}^*(1-\zeta)}{k_2/\rho_T^* + C_{B0}/H\zeta} < 0 \tag{50}$$

where k_1 and k_2 are the first and second components of the matrix $\boldsymbol{K}$, respectively. Notice that, for a given ρ_T^*, $\Delta\bar{a}$ is bounded by an upper line $\mathcal{L}_U$ and a lower line $\mathcal{L}_L$ of positive slopes. Figure 2 shows these lines (dashed–dotted) for arbitrary (but typical) values of the parameters of the inequality [Eq. (46)] (namely, $C_D = 2.2$, $C_{B0}^* = 0.0134$ m^2/kg, $S_1 = 0.06$ m^2, $S_2 = 0.01$ m^2, $m = 5$ kg, $k_1 = -1.830310^{-10}1$/km, $k_2 = 1.854210^{-10}1$/km^2, $H = 58.5150$ km, and $\rho_T^* = 2.56310^{-12}$ kg/m^3) corresponding to an altitude of 421.87 km ([1] p. 564). For the following explanation, the zone in between $\mathcal{L}_U$ and $\mathcal{L}_L$ will be referred to as the nonsaturated zone. Moreover, Fig. 2 also illustrates the solid line $\mathcal{O}$ that satisfies $\Delta\dot{\bar{a}} = 0$. This line is obtained by solving $k_1\Delta\bar{\theta} + k_2\Delta\bar{a} = 0$. The slope of this line is $-k_1/k_2 > 0$, and it passes through the origin. Above(below) $\mathcal{O}$, $\Delta\dot{\bar{a}} < (>)0$. Furthermore, notice that above(below) the line $\Delta\bar{a} = 0$, $\Delta\dot{\bar{\theta}} < (>)0$.

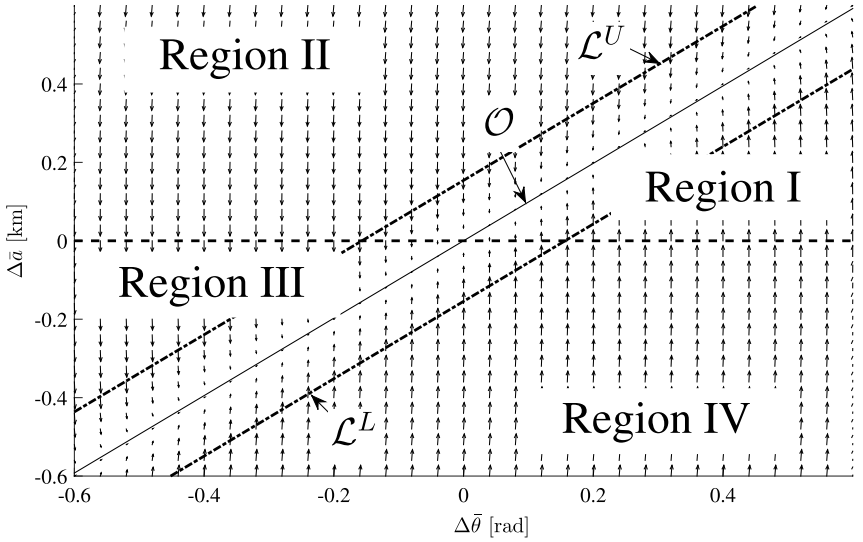

Fig. 2 Phase portrait of the system, depicted with Eqs. (51–53).

Notice that the line $\mathcal{O}$ does not constitute an equilibrium of the system, as only $\Delta\dot{\bar{a}}$ vanishes on it but not $\Delta\dot{\bar{\theta}}$. The only equilibrium of the system is at the origin of the plane $\Delta\bar{\theta} - \Delta\bar{a}$.

According to Eq. (16), there are two necessary conditions that must hold in order to be able to generate differential drag for control purposes. These conditions are formulated as $-\rho_C^* + \rho_T^*\zeta < 0$ and $-\rho_C^*\zeta + \rho_T^* > 0$. If one of these conditions does not hold, $\Delta\bar{a}$ could not be generated in both directions: positive and negative. Considering Eq. (45), these conditions entail the following requirements: $1 > \zeta + \Delta\bar{a}/H$ and $1 > \zeta(1 - \Delta\bar{a}/H)$. As was previously mentioned, the expected values of $\Delta\bar{a}$ are sufficiently small to avoid high natural drift rates from which, for the purposes of this work, they can be assumed as $|\Delta\bar{a}| \leq 10$ km. Moreover, for three units (3U) or longer cubesats, $\zeta = \cos(\pi/2 - \psi) \leq 0.32$. Hence, $1 > \zeta + \Delta\bar{a}/H$ and $1 > \zeta(1 - \Delta\bar{a}/H)$ do not appear difficult to satisfy. It means that, from the viewpoint of the control law (assuming no uncertainties), the differential-drag input $(\rho_C^* u_C^* + \rho_T^* u_T^*)$ can be generated as both positive and negative, as possibly required by the controller.

If these conditions were not satisfied, the nonsaturated zone would not exist, nor could the line $\mathcal{O}$ be defined.

Figure 2 also depicts the phase portrait of the system [Eq. (18)] driven by Eqs. (40–42). At each point $\boldsymbol{w} = [\Delta\bar{\theta}, \Delta\bar{a}]^\top$, the slope of the flow direction is computed as

$$\frac{\mathrm{d}\Delta\bar{a}}{\mathrm{d}\Delta\bar{\theta}} = \frac{\Delta\dot{\bar{a}}}{\Delta\dot{\bar{\theta}}}$$

In the nonsaturated zone, the slope of the flow direction is given by

$$\frac{\mathrm{d}\Delta\bar{a}}{\mathrm{d}\Delta\bar{\theta}} = \frac{b}{P_0}\left(k_1\frac{\Delta\bar{\theta}}{\Delta\bar{a}} + k_2\right) \tag{51}$$

whereas out of this region, the slopes are given by

$$\begin{aligned}\frac{\mathrm{d}\Delta\bar{a}}{\mathrm{d}\Delta\bar{\theta}} &= -\frac{b}{P_0\Delta\bar{a}}(C_{B0}^*(-\rho_C^* + \rho_T^*\zeta)) \\ &= -\frac{bC_{B0}^*\rho_T^*(\zeta - (1 - \Delta\bar{a}/H))}{P_0\Delta\bar{a}}, \qquad \text{if } \boldsymbol{w} \text{ isabove } \mathcal{L}^U\end{aligned} \tag{52}$$

and

$$\begin{aligned}\frac{\mathrm{d}\Delta\bar{a}}{\mathrm{d}\Delta\bar{\theta}} &= -\frac{b}{P_0\Delta\bar{a}}(C_{B0}^*(-\rho_C^*\zeta + \rho_T^*)) \\ &= -\frac{bC_{B0}^*\rho_T^*(-\zeta(1 - \Delta\bar{a}/H) + 1)}{P_0\Delta\bar{a}}, \qquad \text{if } \boldsymbol{w} \text{ isabove } \mathcal{L}^U\end{aligned} \tag{53}$$

The line defined as $\Delta\bar{a} = 0$ along with the line $\mathcal{O}$ determine four regions of the phase portrait, each of which has a distinctive flow direction. These regions are named I, II, III, and IV. In region I, the flow has $\Delta\dot{\bar{a}} > 0$ and $\Delta\dot{\bar{\theta}} < 0$. In region II, the flow evolves such that $\Delta\dot{\bar{a}} < 0$ and $\Delta\dot{\bar{\theta}} < 0$. In region III, the flow is characterized by $\Delta\dot{\bar{a}} < 0$ and $\Delta\dot{\bar{\theta}} > 0$. Finally, in region IV, the flow moves with $\Delta\dot{\bar{a}} > 0$ and $\Delta\dot{\bar{\theta}} > 0$. Each of these regions has a subregion within the nonsaturated zone, denoted by $(\cdot)^{\mathcal{N}}$, and a subregion that is outside the nonsaturated zone, which is denoted by $(\cdot)^{\mathcal{S}}$. Hence, for instance, region I outside(inside) the nonsaturated zone will be referred to as $\mathrm{I}^{\mathcal{S}(N)}$.

As time elapses, considering the slow decay of $\bar{a}_T$ and consequent growth of ρ_T^*, the slopes outside the nonsaturated zone become steeper, as seen from Eqs. (52) and (53). Due to the flow directions of regions $\mathrm{I}^{\mathcal{S}}$ and $\mathrm{III}^{\mathcal{S}}$, the trajectories will eventually reach the nonsaturated zone. In region $\mathrm{IV}^{\mathcal{S}}$, as long as

$$\frac{\mathrm{d}\Delta\bar{a}}{\mathrm{d}\Delta\bar{\theta}} > S_L \tag{54}$$

the trajectories will reach either region $\mathrm{V}^{\mathcal{N}}$ or region $\mathrm{I}^{\mathcal{S}}$; in which case, they also end up at the nonsaturated zone. Inequality (54) entails

$$\Delta\bar{a} > \frac{\zeta - 1}{P_0 S_L/bC_{B0}^*\rho_T^* + \zeta/H} \tag{55}$$

and, with the same typical values used to build Fig. 2, inequality (54) is satisfied as long as $\Delta\bar{a} > -22.03$ km. In region $\mathrm{II}^{\mathcal{S}}$, as long as

$$\frac{\mathrm{d}\Delta\bar{a}}{\mathrm{d}\Delta\bar{\theta}} > S_U \tag{56}$$

the trajectories will flow toward region $\mathrm{II}^{\mathcal{N}}$ or $\mathrm{III}^{\mathcal{S}}$; in which case, they will eventually reach the nonsaturated zone as well. Condition (56) implies

$$\Delta\bar{a} < \frac{1 - \zeta}{P_0 S_U/bC_{B0}^*\rho_T^* + 1/H} \tag{57}$$

With the same values used to build Fig. 2, inequality (56) is satisfied as long as $\Delta\bar{a} < 16.06$ km. For practical purposes, and due to the aforesaid reasons, the value of $|\Delta\bar{a}|$ is expected to be significantly smaller than ∼16 km. Since the phase portrait shows that, due to the controller action, the trajectories always move toward and eventually enter the nonsaturated zone, they cannot leave once they have reached it. Actually, due to the controller, the nonsaturated region constitutes an invariant set. Moreover, once the trajectories are

within the nonsaturated zone, the LQR controller drives the system toward the origin, with no saturation.

Under the presence of uncertainties, the input of the system is given by Eq. (31). Then, η can actually affect the slopes of the flow directions. To measure these effects, consider the following:

$$\Delta\dot{\bar{a}} = b(\nu_{\text{des}} + \eta) \tag{58}$$

although η does not explicitly affect $\Delta\dot{\bar{\theta}} = -P_0\Delta\bar{a}$. As stated by Eq. (54), if in region IV^S the slopes $\mathrm{d}\Delta\bar{a}/\mathrm{d}\Delta\bar{\theta} = \Delta\dot{\bar{a}}/\Delta\dot{\bar{\theta}}$ are higher than S_L, the system will eventually reach the nonsaturated zone. Hence,

$$\Delta\dot{\bar{\theta}}S_L < \Delta\dot{\bar{a}} \quad - P_0\Delta\bar{a}S_L < bC^*_{B0}(-\rho^*_C\zeta + \rho^*_T + \eta) \tag{59}$$

for any η. If

$$|\eta| \le \bar{\eta} < \rho^*_T\left(1 - \zeta\left(1 - \frac{\Delta\bar{a}}{H}\right)\right) + \frac{P_0\Delta\bar{a}S_L}{bC^*_{B0}} \tag{60}$$

holds, as previously mentioned, the trajectories will reach either region IV$^{\mathcal{N}}$ or region I^S; in which case, they also end up at the nonsaturated zone. For region II^S, since $\Delta\dot{\bar{\theta}} < 0$,

$$\Delta\dot{\bar{\theta}}S_U > \Delta\dot{\bar{a}} \quad - P_0\Delta\bar{a}S_U > bC^*_{B0}(-\rho^*_C + \rho^*_T\zeta + \eta) \tag{61}$$

for any η. If

$$|\eta| \le \bar{\eta} < \rho^*_T\left(1 - \zeta - \frac{\Delta\bar{a}}{H}\right) - \frac{P_0\Delta\bar{a}S_U}{bC^*_{B0}} \tag{62}$$

holds. As previously mentioned, the trajectories will reach either region II$^{\mathcal{N}}$ or region III^S; in which case, they also end up at the nonsaturated zone. Numerical values of the expressions involved in the inequalities will be shown in Sec. IV.

E. Computation of β_C and β_T

Using Eqs. (40–42), the angles β_C and β_T are determined. If the system is within the nonsaturated zone, then β_C and β_T must satisfy Eq. (42), which constitutes a single equation with two unknowns. To minimize the orbital decay, it is sought that the cross-sectional areas are always as small as possible. Therefore, one of the angles may be arbitrarily set to yield the minimum possible cross-sectional area, and the other one may be determined to solve Eq. (42). Hence, the following algorithm is proposed to determine β_C and β_T:

$$\begin{cases} \beta_C = 90\ \text{deg} \ \text{ and } \ \beta_T = 90\ \text{deg}, & \text{if } \bar{a}_C = \bar{a}_T \ \text{ and } \ \bar{\theta}_C = \bar{\theta}_T \\ \beta_C = 90\ \text{deg} \ \text{ and } \ \beta_T = \arccos & \text{if } -\boldsymbol{K}\boldsymbol{w} \ge 0 \\ \beta_T = 90\ \text{deg} \ \text{ and } \ \beta_C = \arccos & \text{otherwise} \end{cases} \tag{63}$$

IV. Numerical Simulations

The developed control law was tested in a few simulations. The scenarios were built such that they included realistic effects that affected the dynamics of LEO satellites while maneuvering based on DD. Five simulations will be elaborated here. They will be referred to as cases, and they are summarized in Table 1.

Table 1 Summary of the cases simulated

Case no.	C_D	Corotation	Zonal harmonics	$\bar{i}_{C/T}$, deg	Gains $\tilde{q}_1 = \tilde{q}_2$
1	2.39	No	Up to J_2	10	$5 \cdot 10^{-17}$
2	2.39	No	Up to J_2	97	$5 \cdot 10^{-17}$
3	Eq. (66)	No	Up to J_2	10	$5 \cdot 10^{-17}$
4	Eq. (66)	$\boldsymbol{v}_{\text{atm}} = \boldsymbol{\Omega}_E \times \boldsymbol{r}$	Up to J_2	97	$5 \cdot 10^{-17}$
5	Eq. (66)	$\boldsymbol{v}_{\text{atm}} = \boldsymbol{\Omega}_E \times \boldsymbol{r}$	Up to J_2	97	$5 \cdot 10^{-19}$

Every case implements the density model NRLMSISE-00 [31] as the true density field (hence giving ρ_C and ρ_T), considering the corresponding variations of the F10.7 solar flux index as well as the geomagnetic index AP. To that end, the values of these indices were retrieved from NASA/Goddard Space Flight Center's Operating Missions as Nodes on the Internet (OMNI) database through OMNIWeb.[§] The data were retrieved for the entire years of 2009 through 2011. The presented simulations started on 11 January 11 2010 at 12:23:00 Universal Time (UT) and, with the retrieved data, they could not extend beyond 31 December 2011 at 23:59:59 UT, since simulations with realistic indices were pursued. On the other hand, the density models that were assumed as known by the controllers, ρ^*_C and ρ^*_T, were set as $\rho^*_C = \rho^*_T = 1.1 \cdot 10^{-12}$ kg/m^3, which were arbitrarily set according to the density behavior for 2009 as modeled by NRLMSISE-00. Notice that ρ^*_C and ρ^*_T could be also assumed to have some kinds of variations. Whatever model was assumed for ρ^*_C and ρ^*_T, the bound for the uncertainties $\delta\rho^M$ should have been estimated accordingly if an accurate computation of $\bar{\eta}$ was desired.

NRLMSISE-00 was also used to obtain the true temperature. These temperature values were used to implement the models of drag coefficient variations, as will be elaborated in the following subsections.

For cases 1 and 2, the real drag coefficient C_D was arbitrarily considered to be 2.39 and constant, whereas for other cases, a more realistic model that accounted for the spacecraft attitude, the temperatures of the atmospheres, and the surfaces of the spacecraft, as well as their chemical composition, was simulated. For all the cases, the C^*_D assumed by the controller was set as $C^*_D = 2.2$, generating a realistic amount of uncertainty in this parameter. Moreover, the masses of the satellites were set as 5 kg each, whereas $S_1 = 0.06$ m^2 and $S_2 = 0.01$ m^2.

The simulations were run in Cartesian elements with the corresponding nonlinear differential equations. Since the theoretical developments considered the secular effects generated by the J_2 zonal harmonics, all the simulations included the corresponding J_2 terms in the equations of motion. Moreover, to assess dynamical effects not considered in the development of the LQR, cases 4 and 5 included zonal harmonics terms up to the eighth degree, as well as corotation of the atmosphere, which added more uncertainties than those accounted for in the presented developments.

The equations of motion integrated in the simulations are given by

$$\ddot{\boldsymbol{r}} = \nabla\mathcal{R} - \frac{1}{2m}\rho\|\boldsymbol{v} - \boldsymbol{v}_{\text{atm}}\|(\boldsymbol{v} - \boldsymbol{v}_{\text{atm}})\sum_{i=1}^{3} A_i C_{D_i} \tag{64}$$

where A_i stands for the cross-sectional area of the surface i; and C_{D_i} denotes the drag coefficient corresponding to the same surface, which in general will be considered as functions of the attitude. The velocity of the atmosphere is denoted by $\boldsymbol{v}_{\text{atm}}$. For cases 1, 2, and 3, it is assumed that $\boldsymbol{v}_{\text{atm}} = 0$; whereas for cases 4 and 5, it is assumed that $\boldsymbol{v}_{\text{atm}} = \boldsymbol{\Omega}_E \times \boldsymbol{r}$, where $\boldsymbol{\Omega}_E$ represents the angular velocity of the Earth in an Earth-centered inertial (ECI) frame, assumed to be $\boldsymbol{\Omega}_E = [0, 0, 2\pi/86164.1]^\top$ rad/s: $\boldsymbol{r} = [x, y, z]^\top$ represents the position vector of the satellite in the ECI frame. $\mathcal{R}$ represents the considered geopotential, including zonal harmonics, and is given by ([1] p. 543):

$$\mathcal{R} = \frac{\mu}{r}\left[1 - \sum_{l=2}^{L} J_l\left(\frac{R_{\text{E}}}{r}\right)^l P_l\left(\frac{z}{r}\right)\right] \tag{65}$$

and ∇ is the gradient operator taken in Cartesian coordinates. Moreover, $r = \|\boldsymbol{r}\|$, and $P_l(z/r)$ denotes the Legendre polynomial of the first kind and order l, computed at the ratio z/r.

It is worth mentioning that, in most works and simulations found in the literature dealing with DD maneuvering, the effects due to variations of solar and geomagnetic indices, the corotation of the atmosphere, and the variation of the drag coefficient with the attitude and temperature are neglected. Even simulations performed with Systems Tool Kit (STK®) using the high-precision orbital

[§]Data available online at http://omniweb.gsfc.nasa.gov/.

propagator (HPOP) tend to neglect some of these effects because the HPOP considers a constant C_D.

Since the controllers are formulated in terms of mean orbital elements but the dynamic equations are formulated in Cartesian elements, transformations from mean (osculating) orbital elements to osculating (mean) orbital elements should be implemented. To that end, this work implemented the first-order approximation of the Brouwer theory [32], which for the purpose of this work is seen as a tool to convert from osculating (mean) elements to mean (osculating) representations.

In terms of mean elements, the considered initial conditions are given by $\bar{a}_C(t_0) = 6800$ km, $\bar{e}_C(t_0) = 0.0005$, $\bar{a}_T(t_0) = 6800.01$ km, $\bar{e}_T(t_0) = 0.001$, $\bar{\Omega}_T(t_0) = \bar{\Omega}_C(t_0) = 0$ deg, $\bar{\omega}_T(t_0) = \bar{\omega}_C(t_0) = 0$ deg, $\bar{M}_T(t_0) = 20$ deg, and $\bar{M}_C(t_0) = 0$ deg. Finally, the initial inclinations are specified for each simulation in Table 1. These initial conditions are transformed into the corresponding osculating counterparts and then into Cartesian elements to be integrated. The gains used for the simulations are $\tilde{q}_1 = \tilde{q}_2 = 5 \cdot 10^{-17}$, whereas $a_0 = \bar{a}_T(t_0)$.

For the forthcoming simulations, the depicted results include the time history of $\Delta\bar{\theta}$, $\Delta\bar{a}$, V, β_C, and β_T; ρ_C and ρ_T; ρ_C^* and ρ_T^*; and $\bar{a}_C$ and $\bar{a}_T$. Plots of the distance between the two satellites and out-of-plane coordinate of the relative position vector are shown for cases 4 and 5, in which corotation and J_8 are taken into account. In cases 1, 2, and 3, the behaviors of the distance between the two satellites and the out-of-plane coordinate of the relative position vector are very similar to those shown.

A. Numerical Estimation of the Uncertainty

This section provides an estimation of the uncertainty on the model with respect to the reality defined for the simulations, based on Eq. (36). As previously stated, $\rho_C^* = \rho_T^* = 1.1 \cdot 10^{-12}$ kg/m^3. Considering the assumed ρ^* and according to retrieved data of density for the expected time of the maneuver, $\delta\rho^M$ is considered as $\delta\rho^M = 1.0 \cdot 10^{-12}$ kg/m^3, which represents about 90% of the error in the density model. According to Eq. (17), the maximum value for u_C^* and u_T^* can be stated as $u^{*M} = 0.013382$ m^2/kg. To estimate δu^M, with Eq. (2) and a model for C_{D_i} retrieved from [26–28] that accounts for variations of the drag coefficient due to attitude and temperature, the variations of the ballistic coefficients as a function of the angle β and temperature of the atmosphere are depicted. For completeness, this model will be elaborated on in Sec. IV.C. It is shown in Fig. 3, which also includes the errors with respect to the modeled ballistic coefficient given by $C_{B0}\cos(\beta - \psi)$.

From Fig. 3, it was determined that $\delta u^M = 0.005223$ m^2/kg. Finally, $\bar{\eta} = 4.86966 \cdot 10^{-11}$ 1/km. Recalling, inequalities (60) and (62), considering $\Delta\bar{a}$ up to 4.9 km and with the values corresponding to the forthcoming simulations, the right-hand sides of Eqs. (60) and (62) attain values larger than $\bar{\eta}$, showing that, under the expected uncertainties, the system will converge to the nonsaturated zone. Consider that the inequalities given by Eqs. (60) and (62) are sufficient conditions but not necessary. With the aforementioned values for $\tilde{q}_1$ and $\tilde{q}_2$, the value for expression (39) is obtained as

$$\frac{\|PB\|}{\lambda_{\min}} = 2 \cdot 10^8$$

which means that, as long as $\|\boldsymbol{w}\| > 0.02$, $\dot{V} < 0$. Recall that the involved quantities were adimensionalized using 1 km, 1 rad, 1 kg, and 1 s.

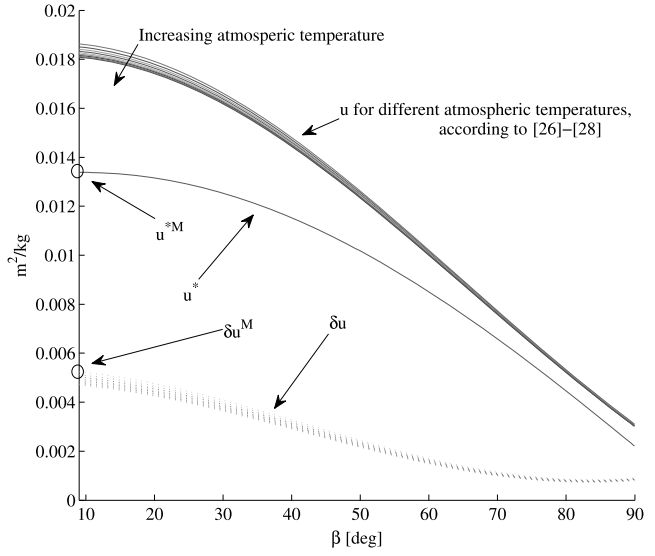

Fig. 3 Variation of u and δu with β and atmospheric temperatures ranging from 700 to 1500 K.

B. Cases 1 and 2

The first two cases consider $C_{D_i} = 2.39$ for every surface of both satellites. The initial mean inclination of case 1 is set as $\bar{i}_T(t_0) = \bar{i}_C(t_0) = 10$ deg; whereas for case 2, it is set as $\bar{i}_T(t_0) = \bar{i}_C(t_0) = 97$ deg. Since DD cannot exert controlled out-of-plane differential specific forces, the simulations are always initiated with same orbital planes for the chaser and target.

For these cases, the parameter L of Eq. (65) is set as two, so it only considers the J_2 zonal harmonic.

The results for case 1 are depicted in Figs. 4 and 5; whereas for case 2, they are plotted in Figs. 6 and 7. The final distances between the

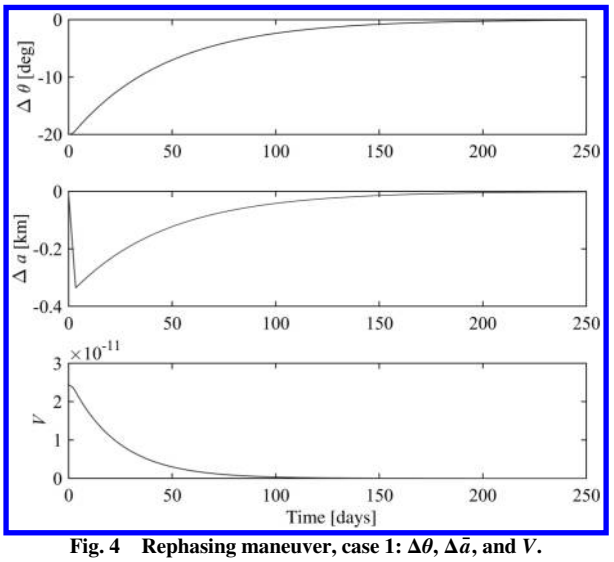

Fig. 4 Rephasing maneuver, case 1: $\Delta\theta$, $\Delta\bar{a}$, and V.

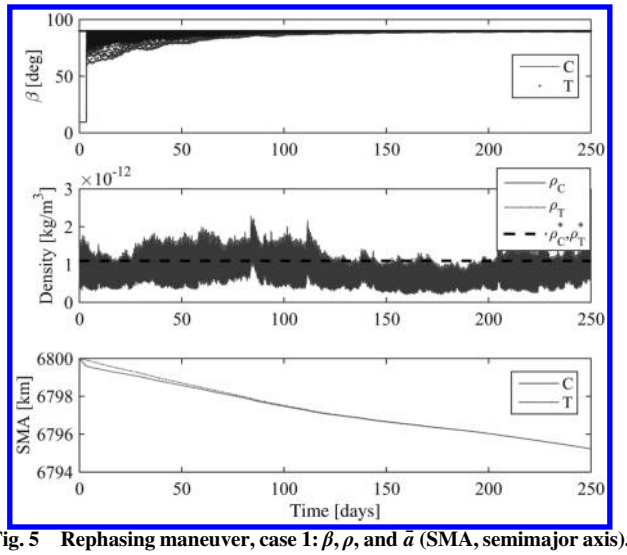

Fig. 5 Rephasing maneuver, case 1: β, ρ, and $\bar{a}$ (SMA, semimajor axis).

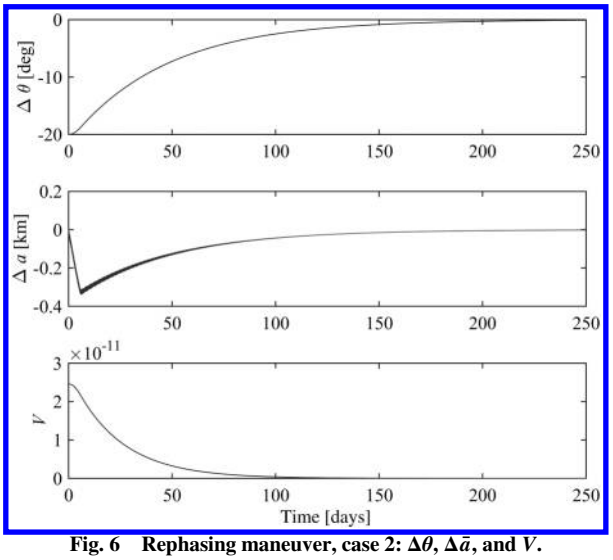

Fig. 6 Rephasing maneuver, case 2: $\Delta\theta$, $\Delta\bar{a}$, and V.

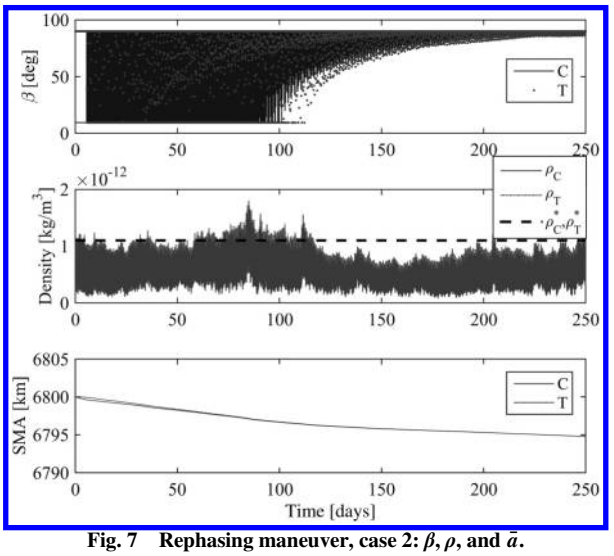

Fig. 7 Rephasing maneuver, case 2: β, ρ, and $\bar{a}$.

two satellites are 25.12 and 6.047 km for cases 1 and 2, respectively; whereas the out-of-plane coordinate oscillated between ± 1.28 and ± 0.90 km for cases 1 and 2, respectively. These oscillations are caused by other perturbations, like zonal harmonics. Differences in the mean semimajor axes generate differences in the rates of change of the right ascensions of the ascending nodes ($\dot{\Omega}_C$ and $\dot{\Omega}_T$), which produce the out-of-plane components.

Figures 4 and 6 show the convergence of the maneuver, as expected from the analysis performed in the previous sections. However, the behaviors of the angles β look different. Case 1 presents less oscillations in β_C and β_T than case 2. Examining the plots of the densities (Figs. 5 and 7: middle plots), it is observed that the differences between the real values of density and the values assumed for tuning the controllers $\delta\rho$ are larger for case II, reaching differences (uncertainties) of 90% during most of the maneuvering time; whereas for case 1, these differences are not so accentuated. These differences are believed to cause the oscillations in the angles β, which in case 2 vary between the extremes of the interval for almost 100 days to overcome the high level of uncertainty in the input. This phenomenon suggests possible difficulties for implementation because of the long intervals with large rotations in the attitude required to attain convergence in the presence of the uncertainties. Improving the models of the density used for the controller, ρ_C^* and ρ_T^*, or fine tuning of the LQR gains could help resulting in a smoother action with lower amplitudes. Although, the latter alternative could enlarge the region around the origin in which stability cannot be guaranteed. Another alternative would be to change the ballistic coefficient by other means than pitching the spacecraft: for example, rotating a set of panels, as the ORBCOMM satellites do [19]. Still, in general, for maneuvers that require a high level of precision in relative position and velocity, this work suggests that DD may not be a feasible alternative because of the need of permanent corrective actions from the controller to compensate for the uncertain models of drag actuation. Yet, for maneuvers or stages of maneuvers with coarse requirements, DD can be very useful.

From Figs. 5 and 7, it is appreciated that the mean semimajor axes, $\bar{a}_C$ and $\bar{a}_T$, undergo a decay of approximately 5 km, validating the linearization proposed in Sec. III.A.

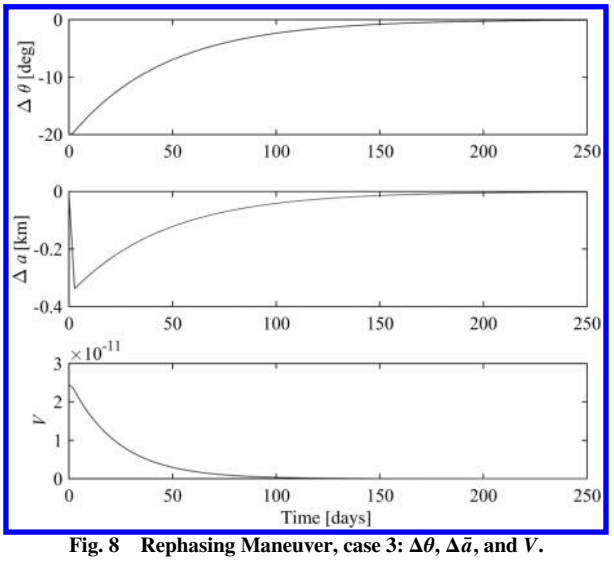

Fig. 8 Rephasing Maneuver, case 3: $\Delta\theta$, $\Delta\bar{a}$, and V.

C. Case 3

The main purpose of this case is to introduce a more realistic model of the drag coefficient in the assumed true dynamics, which varies with the attitude and temperature. In fact, case 3 differs from case 1 only in the manner that the real drag coefficient is modeled. Still, C_D^* assumed by the controller was set as $C_D^* = 2.2$. The same initial inclination as case 1 is considered, i.e., $\bar{i}_T(t_0) = \bar{i}_C(t_0) = 10$ deg.

Based on works [26–28], the drag coefficient of each surface is modeled as

$$C_{D_i} = 2\left(1 + \frac{2}{3}\sqrt{1 + \alpha^i\left(\frac{T^i_{\text{sat}}}{T_{\text{atm}}} - 1\right)}\,\sin\phi_i\right) \tag{66}$$

where

$$\alpha^i = \frac{3.6u^i}{(1+u^i)^2} \tag{67}$$

T^i_{sat} denotes the temperature of the satellite surface i, T_{atm} represents the kinetic temperature of the ambient gas molecules, and u_i is the ratio of the mean mass of the incident gas atom to the mass of the surface atom of the surface i. For the purposes of this work, the aforementioned parameters were set as $T^i_{\text{sat}} = 273$ k (as done in [27,28]), and the temperature T_{atm} was obtained from the NRLMSISE-00 model, with the corresponding F10.7 and AP indices. The angle of attack of the ith surface is represented by ϕ_i, which in fact varies with β. Finally, $u_i = 0.215$ is arbitrarily set, assuming a mean mass of the incident gas atom of 15 (nitrogen and oxygen atoms) and a mean mass of the atoms of the satellite surface to be 69.7, corresponding to gallium solar panels.

The results obtained from this simulation are depicted in Figs. 8 and 9. The obtained behaviors look very similar to those corresponding to case 1, suggesting that the performance of the controller is not significantly affected by the incorporation of a more realistic model of the true C_D behavior, which varies with the attitude and temperature. The final distance between the two satellites is 22.59 km, and the out-of-plane coordinate oscillated ± 1.28 km.

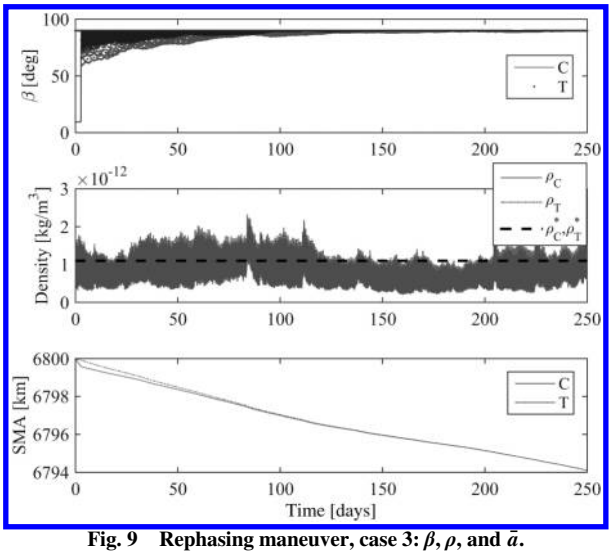

Fig. 9 Rephasing maneuver, case 3: β, ρ, and $\bar{a}$.

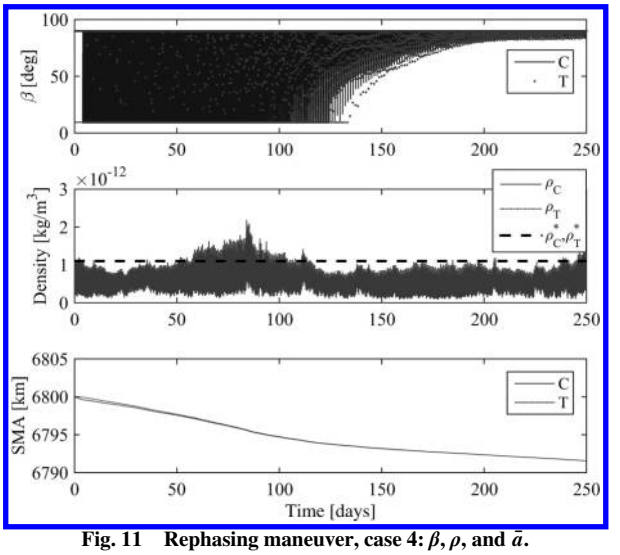

Fig. 11 Rephasing maneuver, case 4: β, ρ, and $\bar{a}$.

D. Case 4

The purpose of this simulation is to assess the effects of the corotational motion of the atmosphere and zonal harmonics, including up to the eighth degree. Hence, the corotation is added by considering $\boldsymbol{v}_{\text{atm}} = \boldsymbol{\Omega}_E \times \boldsymbol{r}$, where $\boldsymbol{\Omega}_E = [0, 0, 2\pi/86164.1]^{\top}$ rad/s. The initial inclination was set as $\bar{i}_T(t_0) = \bar{i}_C(t_0) = 97$ deg.

Since the corotational motion of the atmosphere is considered, and the pitch axis is perpendicular to the plane of motion, it is necessary to consider the drag generated by the impinging particles of the atmosphere onto the lateral faces of the satellites. Hence, there will be an out-of-plane drag force, corresponding to the components of the vector $\boldsymbol{v} - \boldsymbol{\Omega}_{\text{atm}} \times \boldsymbol{r}$ perpendicular to $\boldsymbol{v}$. The surface of each lateral face of the satellite was assumed as $S_3 = 0.06\ \text{m}^2$, like S_1. Furthermore, the variations of the drag coefficients with attitude and temperature are modeled, whereas $C_D^* = 2.2$.

The results of the simulation are shown in Figs. 10–12. it is observed that adding the corotation and more terms of the zonal harmonics series to the real dynamics actually generates larger oscillations of the angles β_C and β_T, which seem to be required to counteract the effects due to the added perturbations. This effect can be also associated to the implementation of the first-order model of the Brouwer transformation, which only considers first-order J_2 terms. Hence, it may not be able to remove oscillations in the orbital elements caused by higher zonal harmonics, which make the angles β to increase their oscillations. Still, under the level of uncertainty in the density and drag coefficients, and the unconsidered perturbations in the dynamical models, the controller performs satisfactorily, driving the two satellites to the expected encounter.

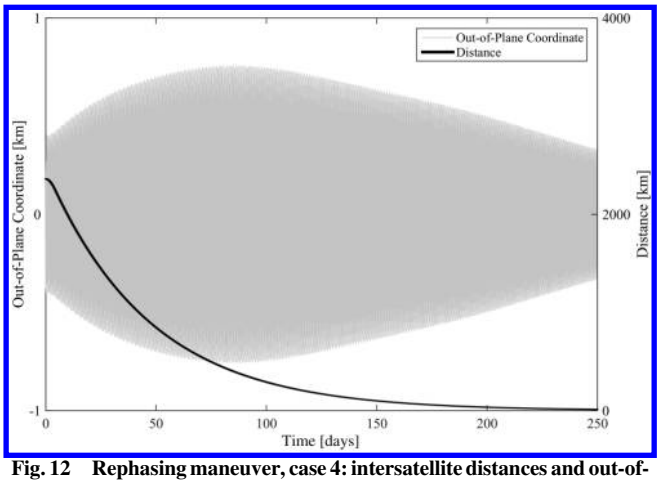

Fig. 12 Rephasing maneuver, case 4: intersatellite distances and out-of-plane coordinate.

E. Case 5

The purpose of this case is to reduce the oscillations of angles β_C and β_T by using smaller gains for the LQR. In this case, $\tilde{q}_1 = \tilde{q}_2$ was set to have a value of $5 \cdot 10^{-19}$, whereas for all the previous cases, they had a value of $5 \cdot 10^{-17}$. Otherwise, this case is identical to case 4.

The results of these simulations are shown in Figs. 13–15. Comparing Figs. 11–14, it is observed that the smaller LQR gains

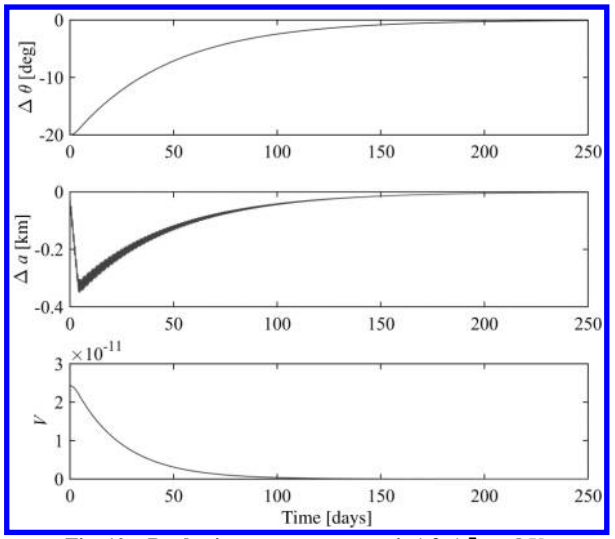

Fig. 10 Rephasing maneuver, case 4: $\Delta\theta$, $\Delta\bar{a}$, and V.

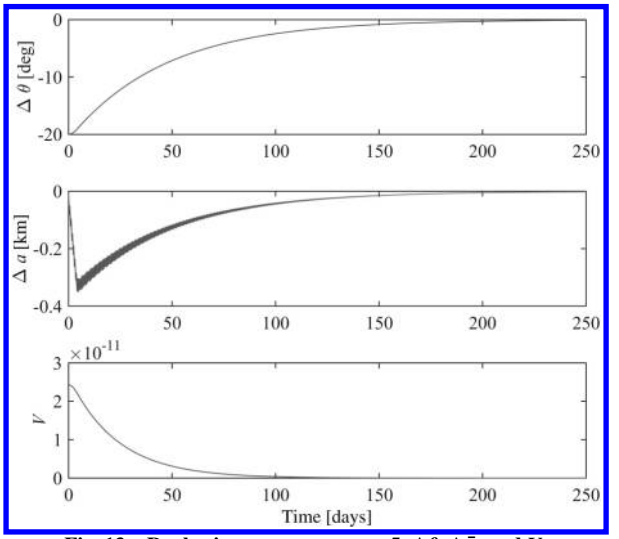

Fig. 13 Rephasing maneuver, case 5: $\Delta\theta$, $\Delta\bar{a}$, and V.

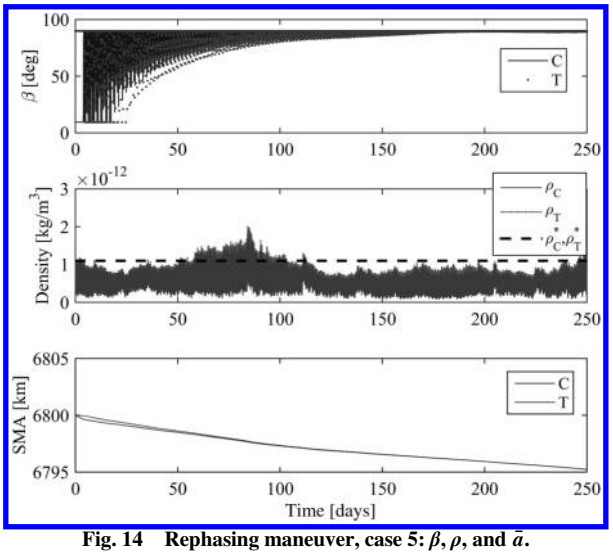

Fig. 14 Rephasing maneuver, case 5: β, ρ, and $\bar{a}$.

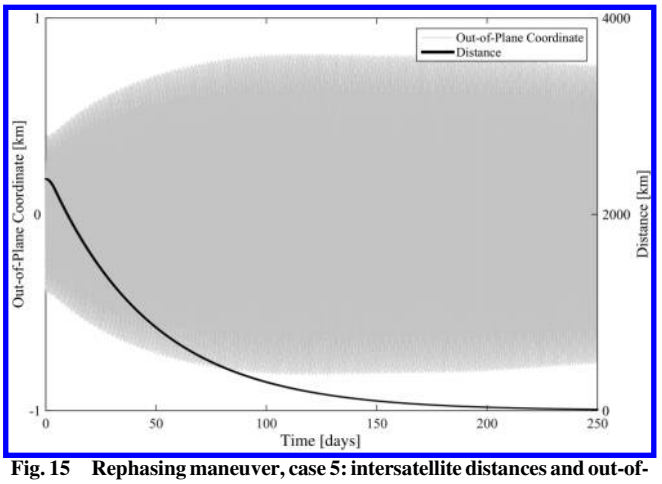

Fig. 15 Rephasing maneuver, case 5: intersatellite distances and out-of-plane coordinate.

result in a faster reduction of the oscillation amplitude of angles β_C and β_T, although the region where the fact that $\dot{V} < 0$ cannot be guaranteed grows. Similar to all the other cases, case 5 shows that, under the level of uncertainty in the density and drag coefficients, as well as the unconsidered perturbations in the dynamical models, the controller also performs satisfactorily, driving the two satellites to the expected encounter.

V. Conclusions

In the last decades, the idea of propellantless spacecraft relative maneuvering via differential drag has received substantial attention. Nevertheless, the explicit inclusion of drag model uncertainties in the control laws has been mostly neglected. This work presented a methodology to perform differential-drag relative maneuvering of coplanar spacecraft, toward rendezvous, under bounded uncertainties in the drag force. The required differential-drag accelerations were obtained by varying the pitch angles of the satellites, thus changing their ballistic coefficients.

The developed approach enables consideration of long-range maneuvers, assuming that both satellites are initially in circular orbits. The developed dynamical system, based on mean semimajor axes and mean arguments of latitude, allows for the implementation of a linear quadratic regulator with a saturation function. In the presence of bounded uncertainties, convergence of the trajectories can be proved up to a certain norm of the state vector, for which an analytical expression is provided in terms of the uncertainties. The effect of saturation in the control is examined by analyzing the phase portrait of the closed-loop dynamics, which shows that the system will eventually desaturate, and hence converge.

Several simulations were presented, including realistic effects like variation of the drag coefficients with the attitude and temperature, the density field given by NRLMSISE-00 with realistic solar flux and geomagnetic indices behavior, and corotation of the atmosphere and zonal harmonics. The simulations consistently showed convergence of the maneuvers, illustrating the robustness of the approach under actual uncertainties and modeling errors, supporting the analytical developments.

An interesting natural extension of this work would consider lift forces and three-dimensional attitude variations to examine the possibility of controlling the out-of-plane relative motion of the satellites, which could also be relevant to maneuver spacecraft that lose the propulsion system due to failures and/or propellant depletion.

Acknowledgments

The authors wish to thank the University of Florida and the U.S. Air Force Office of Scientific Research (contract no. N00014-15-1-2087) for supporting this research. This work was initiated during Fabio Curti's visit to the University of Florida in the Spring of 2015.

References

[1] Vallado, D. A., *Fundamentals of Astrodynamics and Applications*, McGraw–Hill, New York, 2007, pp. 543, 549, 564, 671.

[2] Finley, T., Rose, D., Nave, K., Wells, W., Redfern, J., Rose, R., and Ruf, C., "Techniques for LEO Constellation Deployment and Phasing Utilizing Differential Aerodynamic Drag," *Advances in the Astronautical Sciences*, American Astronomical Soc. Paper 2013-797, Washington, D.C., 2013.

[3] Kumar, B. S., and Ng, A., "A Bang-Bang Control Approach to Maneuver Spacecraft in a Formation with Differential Drag," *AIAA Guidance, Navigation, and Control Conference and Exhibit*, AIAA Paper 2008-6469, 2008. doi:10.2514/6.2008-6469

[4] Leonard, C., "Formation Keeping of Spacecraft via Differential Drag," M.S. Thesis, Massachusetts Inst. of Technology, Cambridge, MA, July 1986.

[5] Leonard, C., Hollister, W., and Bergmann, E., "Orbital Formation Keeping with Differential Drag," *Journal of Guidance, Control, and Dynamics*, Vol. 12, No. 1, 1989, pp. 108–113. doi:10.2514/3.20374

[6] Clohessy, W. H., and Wiltshire, R. S., "Terminal Guidance System for Satellite Rendezvous," *Journal of the Aerospace Sciences*, Vol. 27, No. 9, 1960, pp. 653–658. doi:10.2514/8.8704

[7] Carter, T., and Humi, M., "Clohessy–Wiltshire Equations Modified to Include Quadratic Drag," *Journal of Guidance, Control, and Dynamics*, Vol. 25, No. 6, 2002, pp. 1058–1063. doi:10.2514/2.5010

[8] Bevilacqua, R., and Romano, M., "Rendezvous Maneuvers of Multiple Spacecraft Using Differential Drag under J2 Perturbation," *Journal of Guidance, Control, and Dynamics*, Vol. 31, No. 6, 2008, pp. 1595–1607. doi:10.2514/1.36362

[9] Bevilacqua, R., Hall, J. S., and Romano, M., "Multiple Spacecraft Rendezvous Maneuvers by Differential Drag and Low Thrust Engines," *Celestial Mechanics and Dynamical Astronomy*, Vol. 106, No. 1, 2010, pp. 69–88. doi:10.1007/s10569-009-9240-3

[10] Schweighart, S. A., and Sedwick, R. J., "High-Fidelity Linearized J Model for Satellite Formation Flight," *Journal of Guidance, Control, and Dynamics*, Vol. 25, No. 6, 2002, pp. 1073–1080. doi:10.2514/2.4986

[11] Pérez, D., and Bevilacqua, R., "Differential Drag Spacecraft Rendezvous Using an Adaptive Lyapunov Control Strategy," *Acta Astronautica*, Vol. 83, Feb.–March 2013, pp. 196–207. doi:10.1016/j.actaastro.2012.09.005.

[12] Ben-Yaacov, O., and Gurfil, P., "Long-Term Cluster Flight of Multiple Satellites Using Differential Drag," *Journal of Guidance, Control, and Dynamics*, Vol. 36, No. 6, 2013, pp. 1731–1740. doi:10.2514/1.61496

[13] Ben-Yaacov, O., and Gurfil, P., "Stability and Performance of Orbital Elements Feedback for Cluster Keeping Using Differential Drag,"

Journal of the Astronautical Sciences, Vol. 61, No. 2, 2014, pp. 198–226.
doi:10.1007/s40295-014-0022-0

[14] Schaub, H., "Incorporating Secular Drifts into the Orbit Element Difference Description of Relative Orbits," *13th AAS/AIAA Space Flight Mechanics Meeting*, American Astronautical Soc. Paper 2003-115, 2003, pp. 239–257.

[15] Harris, M. W., and Açkmeşe, B., "Minimum Time Rendezvous of Multiple Spacecraft Using Differential Drag," *Journal of Guidance, Control, and Dynamics*, Vol. 37, No. 2, 2014, pp. 365–373.
doi:10.2514/1.61505

[16] Dell'Elce, L., and Kerschen, G., "Comparison Between Analytical and Optimal Control Techniques in the Differential Drag Based Rendez-Vous," *Proceedings of the 5th International Conference on Spacecraft Formation Flying Missions & Technologies*, 2013, www.sffmt2013.org/PPAbstract/4039p.pdf [retrieved 2016].

[17] Dell'Elce, L., Martinusi, V., and Kerschen, G., "Robust Optimal Rendezvous Using Differential Drag," *Astrodynamics Specialist Conference*, AIAA Paper 2014-4161, 2014.
doi:10.2514/6.2014-4161

[18] Dell'Elce, L., "Satellite Orbits in the Atmosphere: Uncertainty Quantification, Propagation and Optimal Control," Ph.D. Thesis, Univ. de Liège, Liège, Belgium, 2015.

[19] Maclay, T., and Tuttle, C., "Satellite Stationkeeping of the ORBCOMM Constellation Via Active Control of Atmospheric Drag: Operations, Constraints, and Performance (AAS 05-152)," *Advances in the Astronautical Sciences*, Vol. 120, No. 1, 2005, pp. 763–773.

[20] Vallado, D. A., and Finkleman, D., "A Critical Assessment of Satellite Drag and Atmospheric Density Modeling," *Acta Astronautica*, Vol. 95, Feb.–March 2014, pp. 141–165.
doi:10.1016/j.actaastro.2013.10.005

[21] Mishne, D., "Formation Control of Satellites Subject to Drag Variations and J_2 Perturbations," *Journal of Guidance, Control, and Dynamics*, Vol. 27, No. 4, 2004, pp. 685–692.
doi:10.2514/1.11156.

[22] Schaub, H., Vadali, S. R., Junkins, J. L., and Alfriend, K. T., "Spacecraft Formation Flying Control Using Mean Orbit Elements," *Journal of the Astronautical Sciences*, Vol. 48, No. 1, 2000, pp. 69–87.

[23] Schaub, H., and Alfriend, K. T., "Impulsive Feedback Control to Establish Specific Mean Orbit Elements of Spacecraft Formations," *Journal of Guidance, Control, and Dynamics*, Vol. 24, No. 4, 2001, pp. 739–745.
doi:10.2514/2.4774

[24] Mazal, L., and Gurfil, P., "Closed-Loop Distance-Keeping for Long-Term Satellite Cluster Flight," *Acta Astronautica*, Vol. 94, No. 1, 2014, pp. 73–82.
doi:10.1016/j.actaastro.2013.08.002

[25] Battin, R., *An Introduction to the Mathematics and Methods of Astrodynamics*, AIAA Education Series, AIAA, Reston, VA, 1999, p. 489.
doi:10.2514/4.861543

[26] Cook, G., "Satellite Drag Coefficients," *Planetary and Space Science*, Vol. 13, No. 10, 1965, pp. 929–946.
doi:10.1016/0032-0633(65)90150-9

[27] Bruinsma, S., Tamagnan, D., and Biancale, R., "Atmospheric Densities Derived from CHAMP/STAR Accelerometer Observations," *Planetary and Space Science*, Vol. 52, No. 4, 2004, pp. 297–312.
doi:10.1016/j.pss.2003.11.004

[28] Sutton, E. K., Nerem, R. S., and Forbes, J. M., "Density and Winds in the Thermosphere Deduced from Accelerometer Data," *Journal of Spacecraft and Rockets*, Vol. 44, No. 6, 2007, pp. 1210–1219.
doi:10.2514/1.28641

[29] Kwakernaak, H., and Sivan, R., *Linear Optimal Control Systems*, Vol. 1, Wiley-Interscience, New York, 1972, Chap. 3.3.

[30] Khalil, H. K., *Nonlinear Systems*, Prentice–Hall, Upper Saddle River, NJ, 2000, Chap. 4.

[31] Picone, J., Hedin, A., Drob, D. P., and Aikin, A., "NRLMSISE-00 Empirical Model of the Atmosphere: Statistical Comparisons and Scientific Issues," *Journal of Geophysical Research: Space Physics (1978–2012)*, Vol. 107, No. A12, 2002, pp. SIA 15-1–SIA 15-16.
doi:10.1029/2002JA009430

[32] Schaub, H., and Junkins, J., *Analytical Mechanics of Aerospace Systems*, Vol. 1, AIAA, Reston, VA, 2003, Appendix F, pp. 693–696.